PNAS RESEARCH ARTICLE | MEDICAL SCIENCES OPEN ACCESS

Germline variants in *UHRF1* are associated with multilocus imprinting disturbance in humans and mice

Eguzkine Ochoa[a,1], Ilona Zvetkova[b,1], Sunwoo Liv Lee[a], Nozomi Takahashi[c], Benoit Lan-Leung[a], Emma Hobson[d], Mahmoud Issa[d], Bryndis Yngvadottir[a], France Docquier[a,e], Fay Rodger[a,e], Dounia Foster-Hall[f], Graeme Clark[a,e], Ana Toribio[a,e], Ezequiel Martin[a,e], Leonardo Bottolo[a,g,h], Anne C. Ferguson-Smith[c], Wolfgang Fischle[i], Miguel Constancia[b,f,j,1,2], and Eamonn R. Maher[a,k,1,2]

Affiliations are included on p. 7.

Edited by Arthur Beaudet, Luna Genetics, Inc., Houston, TX; received March 19, 2025; accepted May 19, 2025

The investigation of congenital imprinting disorders (CIDs) provides opportunities to elucidate the molecular mechanisms and role of genomic imprinting in development and human disease. Beckwith–Wiedemann spectrum (BWSp) is a prototypic CID resulting from genetic and epigenetic alterations of imprinted genes at chromosome 11p15.5. In up to a quarter of individuals with BWSp, the epigenetic alterations are not confined to 11p15.5 imprinting control regions but also involve other imprinted gene clusters (multilocus imprinting disturbance; MLID). In a consanguineous family with two children diagnosed with BWSp and MLID, the affected individuals were homozygous for a missense variant in *UHRF1*, a gene previously implicated in the maintenance of DNA methylation. To investigate whether the *UHRF1* c. 2001G>C, p.(Lys667Asn) missense substitution predisposes to abnormal establishment/maintenance of genomic imprinting patterns, a genetically engineered mouse model with a *Uhrf1* p.(Lys661Asn) variant was developed. Mice homozygous for the variant born to heterozygous mothers did not display an abnormal phenotype, but homozygotes born to healthy homozygous mothers displayed a range of phenotypes including prenatal lethality. Also, MLID was observed in affected mouse embryos. These findings are consistent with biallelic *UHRF1* variants in affected individuals resulting in an autosomal recessively inherited cause of MLID in humans and expand the range of epigenetic disorders associated with *UHRF1*.

methylation | genomic imprinting | congenital imprinting disorder | multilocus imprinting disturbance | inherited

Significance

Genomic imprinting is an epigenetic process crucial for normal development and is disrupted in congenital imprinting disorders (CIDs). There is great interest in the clinical consequences and etiology of multilocus imprinting disturbance (MLID) which occurs in some individuals with CID, though the cause of MLID is unknown in most cases. We investigated a kindred with a CID and MLID and identified a rare genetic variant in the *UHRF1* gene which has a critical role in the establishment and maintenance of DNA methylation. We generated a mouse model and found that the equivalent *Uhrf1* variant was associated with prenatal lethality and disruption of normal imprinting mechanisms. These findings support *UHRF1* as a candidate gene for CIDs with MLID.

Normal embryo development in humans and mice requires exquisite regulation of gene expression through complex mechanisms of epigenetic control that include DNA methylation and variation in chromatin structure and function (1, 2). Patterns of DNA methylation are dynamic during gametogenesis and early embryogenesis and differ between imprinted and nonimprinted loci (1–4). During gametogenesis, there is a genome-wide demethylation (erasure) followed by remethylation. In the case of imprinted loci, the remethylation establishes a parent-of-origin specific pattern of methylation at differentially methylated imprinting control centers [ICs or imprinted differentially methylated regions (iDMRs)] (2, 4). Following fertilization, a wave of demethylation and remethylation occurs at nonimprinted loci. The methylation patterns (and associated parent-of-origin allele-specific patterns of chromatin structure and modifications) established at iDMRs are maintained throughout life in all somatic cells (2, 4, 5).

It has been estimated that there are ~150 imprinted genes in humans (including those which demonstrate tissue specific imprinting). Imprinted genes have been preferentially linked to roles in growth, metabolism, and development (2, 6). Congenital imprinting disorders (CIDs) are a group of overlapping conditions that result from disordered expression or function of single or multiple imprinted genes and include prototypic disorders such as Angelman syndrome, Beckwith–Wiedemann spectrum (BWSp), Prader–Willi syndrome, and Silver–Russell syndrome (SRS) (7, 8). A variety of mechanisms may cause CIDs including single-gene pathogenic variants, structural variants, uniparental disomy, and epimutations, though the frequency of the individual molecular causes varies between disorders. For example, in BWSp and SRS, epimutations (i.e., loss or gain of methylation (LOM/GOM) at an iDMR) are the most common finding (9–11). Epimutations usually occur at a single iDMR but in a subset of individuals with CIDs multiple iDMRs may be involved (known as multilocus imprinting disturbance, MLID) (12, 13). Epimutations may arise from a failure to establish and/or maintain the appropriate iDMR methylation pattern. Although the cause of MLID is unknown in many cases, both environmental (e.g., assisted reproductive technologies such as embryo culture) and genetic factors have

Author contributions: E.O., I.Z., S.L.L., M.C., and E.R.M. designed research; E.O., I.Z., S.L.L., N.T., B.L.-L., B.Y., F.D., F.R., D.F.-H., G.C., A.T., E.M., and M.C. performed research; E.H., M.I., L.B., A.C.F.-S., and W.F. contributed new reagents/analytic tools; E.O., I.Z., S.L.L., N.T., B.L.-L., B.Y., E.M., M.C., and E.R.M. analyzed data; N.T., B.L.-L., E.H., M.I., B.Y., F.D., F.R., D.F.-H., G.C., A.T., E.M., L.B., A.C.F.-S., and W.F. reviewed and edited the manuscript; E.R.M and M.C. supervised the research; and E.O., I.Z., S.L.L., M.C., and E.R.M. wrote the paper.

The authors declare no competing interest.

This article is a PNAS Direct Submission.

[1]E.O., I.Z., M.C., and E.R.M. contributed equally to this work.

[2]To whom correspondence may be addressed. Email: jmasmc2@cam.ac.uk or e.maher@aston.ac.uk.

This article contains supporting information online at https://www.pnas.org/lookup/suppl/doi:10.1073/pnas.2505884122/-/DCSupplemental.

Published August 18, 2025.

been implicated (12–14). In ~50% patients with transient neonatal diabetes mellitus (TNDM), MLID is associated with biallelic loss of function variants in the *ZFP57* gene (15). In addition, women with biallelic pathogenic variants in maternal effect genes (e.g., *NLRP2*, *NLRP5*, *NLRP7*, *OOEP, PADI6,* and *KHDC3L*) that encode subunits of the oocyte subcortical maternal complex (SCMC) can be affected by reproductive failure and pregnancy complications including early pregnancy loss, recurrent hydatidiform moles, and CIDs, such as BWSp, with MLID (16–20). From a clinical perspective, it is important to identify cases of MLID with an underlying genetic cause as the recurrence risks in further pregnancies can range from 25% to up to 100%, depending on the gene/condition involved (13). Hence, a comprehensive knowledge of the genetic basis of MLID is critical both for the management of affected families and to gain insights into the molecular pathogenesis of epimutations. Here, using the results of human and mouse studies, we identify *UHRF1* as a candidate gene for an autosomal recessively inherited cause of MLID in humans.

Results

Clinical Presentation and Family History of Siblings with BWSp. A family with parental consanguinity, two siblings diagnosed with BWSp and two unaffected siblings, was ascertained (Fig. 1*A*). The proband (III-1) was born via Caesarean section (LSCS) at 35 wk due to the presence of polyhydramnios. Her birth weight was 3.29 kg (99th centile), length 49.5 cm (96th centile), and head circumference 33.2 cm (84th centile). Macroglossia and low set ears were noted. There were no episodes of neonatal hypoglycemia. A 5 cm umbilical hernia was present (International BWS Consensus Clinical Score = 4) (10). At age 14 mo (12.75 mo gestation corrected): Weight was 15.84 kg [>99th centile (+5.2 SD)], length 81 cm (98th centile), and head circumference 47.6 cm (96th centile). Other features noted on examination included macrostomia, thin upper lips, bushy eyebrows, synophrys, abnormal crease below lower eye lid, overfolded ear helix, and abnormal inverted nipples. A surgical tongue reduction was performed at 16 mo. The second affected sibling (III-2) was born preterm at 32 wk with macroglossia, divarication of the recti and a horizontal ear crease. Her birth weight was 1.6 kg (37th centile). An umbilical cord hernia and hypoglycemia were observed after delivery. At 5.5 mo (3.5 mo gestation corrected) her head circumference was 40 cm (37th centile), she had earlobe creases, a reduceable umbilical hernia with macroglossia and protruding tongue with left side larger than the right side (International BWS Consensus Clinical Score = 4) (10). At the age of 11 mo, she was seen in the craniofacial clinic for a prominent metopic suture. CT skull reported normal metopic suture fusion.

Routine molecular diagnostic testing for BWSp was performed by methylation sensitive multiplex ligation-dependent probe amplification (MRC Holland) in both siblings and demonstrated loss of maternal allele methylation (LOM) at the IC2 iDMR (*KCNQ1OT1*:TSS DMR) at chromosome 11p15.5 in both affected siblings (LOM at IC2 is found in ~50% of individuals with BWSp).

Detection of Candidate Missense Variant in *UHRF1* by Exome Sequencing. The association of parental consanguinity with familial BWSp suggested a recessive disorder in both siblings or biallelic pathogenic variants in a maternal-effect gene in the mother, and therefore exome sequencing in the mother and both siblings

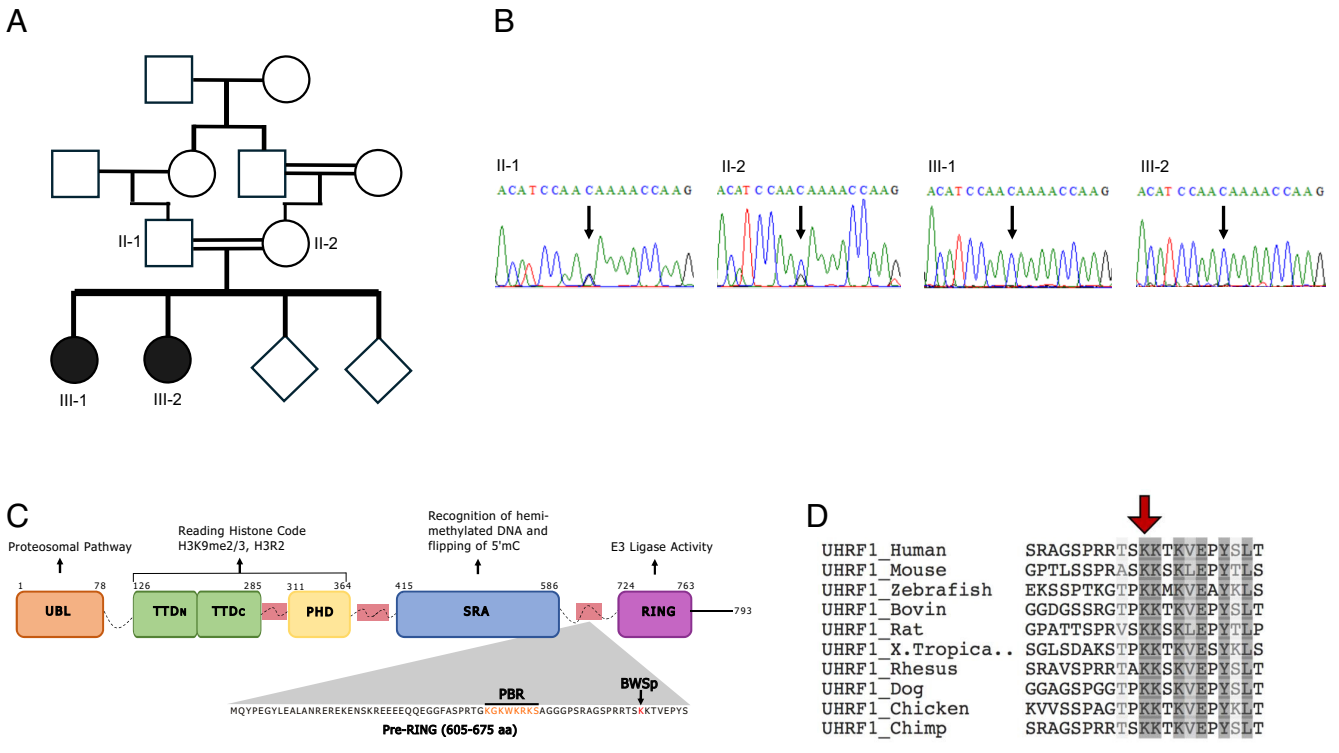

Fig. 1. Clinical and genetics studies of a family with BWSp. (*A*) Family pedigree showing parental consanguinity in the parents (II:1 and II:2) and maternal grandparents (I:1 and I:2) of the two affected siblings (III:1 and III:2). (*B*) Sanger sequencing confirmation of the c. 2001G>C, p.(Lys667Asn) variant that is homozygous in the affected siblings and heterozygous in their parents. (*C*) Location of functional domains in UHRF protein. UBL= ubiquitin-like domain that recognizes and binds to target proteins; TTD—tandem tudor domains that bind trimethylated lysine residues on histone 3; PHD= plant homeodomain finger that binds to unmodified histone H3 tails; SRA= SET and RING-associated domain that binds to hemimethylated DNA; RING finger domain involved in ubiquitinating histones and other proteins. The location of the p.(Lys667Asn) variant on the UHRF1 protein between the SRA and RING domains is indicated; (*D*) conservation of the Lys667 residue across multiple species (21).

was performed. No homozygous candidate pathogenic variants in candidate maternal effect genes (*NLRP2*, *NLRP5*, *NLRP7*, *OOEP, PADI6,* and *KHDC3L*) were identified in the mother or in *ZFP57* or *ZNF445* in the proband. In the two siblings, there were 14 shared protein-altering homozygous variants (12 missense substitutions, one stopgain, and one inframe deletion in 14 unique genes) that passed variant filtering, were present in both siblings and had a maximum allele frequency of <5% [the highest allele frequency observed in any population from 1,000 genomes, ESP or gnomAD (v3.1.2)] (Dataset S1). After variant prioritization and review of the function of the candidate genes, it was concluded that *UHRF1* was the most plausible candidate gene for an autosomal recessively inherited MLID-associated phenotype. *UHRF1* encodes a protein (ubiquitin like with PHD and ring finger domains 1; also known as NP95 or ICBP90) that recognizes and targets DNMT1 to hemimethylated CpG residues (22, 23).

The *UHRF1* missense variant [chr19:4954693 G > C (GRCh38)], NM_001048201.3, c.2001G>C, p.(Lys667Asn) (K667N) was present in a homozygous state in both affected siblings and in a heterozygous state in both parents (Fig. 1*B*). The c. 2001G>C, p.(Lys667Asn) variant was present in the heterozygous state in 1 in 1,613,598 alleles in the Genome Aggregation Database [gnomAD (v4.1.0)] (24). Computational predictions for the variant included deleterious by Mutation Taster (25), deleterious by SIFT (score: 0.015), probably damaging by PolyPhen-2 (score: 0.991), a CADD score of 24 (26–29), REVEL (30) score of 0.078 (functional impact unlikely), and a Meta-EA (31) score of 45.86 (intermediate). The affected amino acid was found to be conserved across a variety of species including mice, zebrafish, and *Xenopus tropicalis* (Fig. 1*D*) and AlphaMissense (32) pathogenicity score was within the likely pathogenic range (score = 0.808; likely pathogenic 0.564 to 1). The K667N substitution did not occur in one of the major functional domains of UHRF1 but within the linker 4 region between the SRA and RING protein domains, 16 amino acids downstream of the PBR regions (Fig. 1*C*).

Identification of MLID in Siblings with BWSp. To determine whether the IC2 LOM was part of a wider disturbance of iDMR methylation status, iDMR (n = 63) methylation profiling was undertaken using a custom targeted methylation sequencing panel (ImprintSeq) (33). The proband (III-1) exhibited significant methylation alterations at 30 of 63 iDMRs. As previously, LOM/GOM events were graded according to the magnitude of the alteration in the DMRs between controls and patients: high methylation alterations (HMAs) and moderate methylation alterations (MMAs) (33). The methylation alterations in the proband included 27 LOM-HMA, 2 GOM-HMA, and 1 GOM-MMA (Fig. 2*A* III-1 and Dataset S2). Affected sibling (III-2) demonstrated significant methylation alterations at 35 iDMRs (31 LOM-HMA, 1 LOM-MMA,1 GOM-HMA, and 2 GOM-MMA (Fig. 2*A* III-2 and Dataset S2). The iDMRs with significant LOM in both affected individuals included IC2 (KCNQ1OT1:TSS), and all LOM iDMRs occurred at primary oocyte gDMRs and GOM in secondary gDMRs and sperm gDMRs (Fig. 2*A* and Dataset S2). Neither parent showed a significant methylation alteration.

Genome-Wide Methylation Profiles with Biallelic *UHRF1* Missense Variants. To explore whether the impact of homozygosity for the *UHRF1* K667N substitution on methylation occurred preferentially at iDMRs or was more widespread, we performed genome-wide methylation profiling with reduced-representation bisulfite sequencing (RRBS) in the proband (III-1) and in six

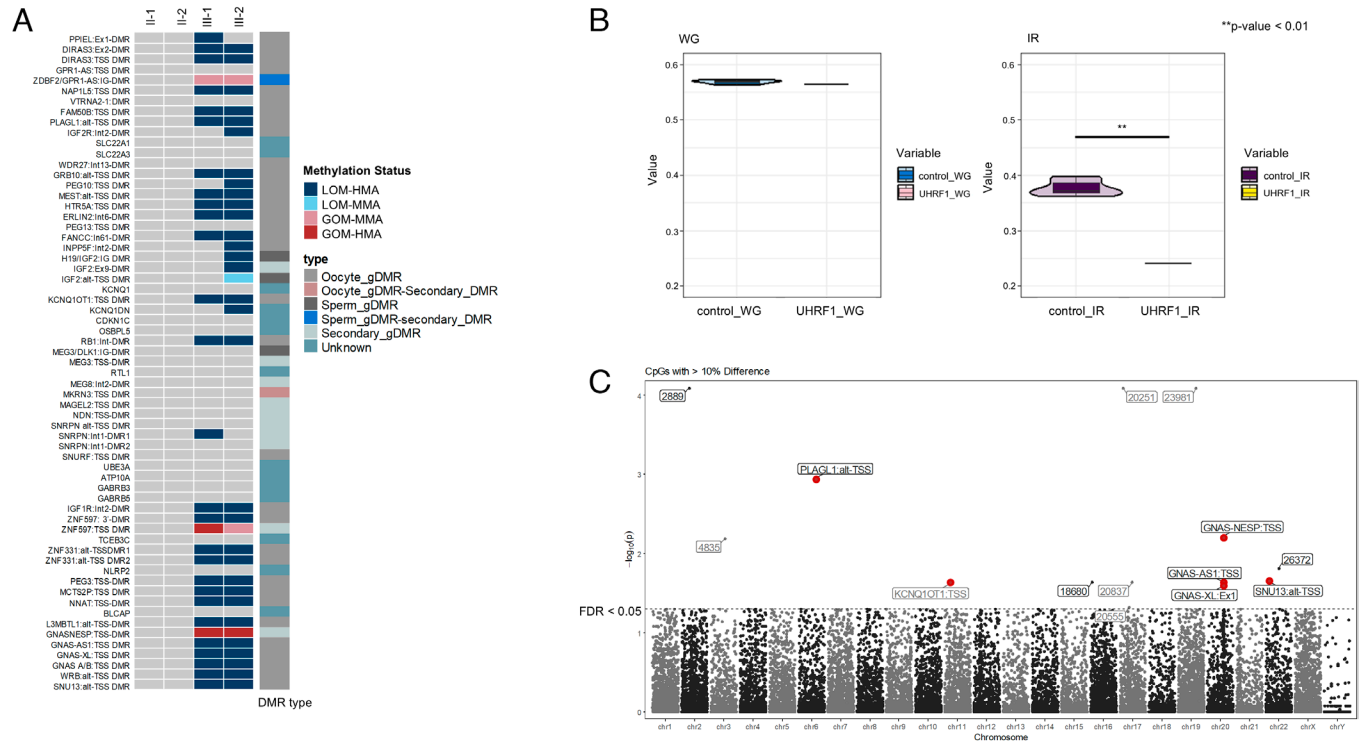

Fig. 2. LOM at imprinted regions (IR) in humans. (*A*) Imprinted region methylation profiles at 63 iDMRs in two affected siblings (III-1 and III-2) and both parents (II-1 and II-2) as assessed by ImprintSeq (33). Significant losses and gain of methylation are indicated with blue representing LOM and red GOM. (*B*) Comparison of methylation levels at IR and nonIR (WG) in proband with homozygous *UHRF1* variant compared to normal controls (n = 6). (*C*) Manhattan plot based on CpGs with a methylation difference of >10%. Significant CpG islands, labeled with an FDR adjusted *P*-value of less than 0.05, were identified based on combined methylation values within the CpG islands. The number and location details of CpG islands are provided in Dataset S2. A total of 14 CpG islands met the threshold, with six of these regions located within IR.

healthy controls. After filtering, 1,674,964 CpGs were included in the analysis. The comparison of DNA methylation profiles between the proband and controls revealed 14 CpG islands, 8 genes, and 9 promoters with significant differential methylation with *P*-value adjusted less than 0.05, level of change greater than 10%, and more than one CpG per region (Dataset S2). This represents 0.0616% (14/22,715) of CpG islands (CpGi), 0.0285% (8/28,054) of annotated genes, and 0.0355% (9/25,386) of promoters that showed significant alterations at DNA methylation level in the proband in comparison with controls. The significant alterations identified in the affected individual were enriched in imprinting-related regions (6/14 CpGi: *PLAGL1:alt-TSS, KCNQ1OT1:TSS, GNAS-NESP:TSS, GNAS-AS1:TSS*, *GNAS-XL:Ex1*, and *SNU13:alt-TSS*). The mean methylation at imprinted regions (IR) showed significant differences between the proband and healthy controls (*P*-unadjusted < 0.01) (Fig. 2 *B*, *Right*); however, overall methylation across the genome was similar (Fig. 2 *B*, *Left*). These results were consistent with the hypothesis that the *UHRF1* K667N variant resulted preferentially in disordered methylation at iDMRs (though methylation alterations were not exclusive to iDMRs). We additionally assessed the statistical significance of the iDMRs by plotting adjusted p-values (-log10(p-adjusted)) and all of six iDMRs demonstrated significant differences when compared to other CpGs. The *PLAGL1:alt-TSS* region exhibited the most significant differences and the *GNAS-NESP:TSS DMR* also showed a highly significant difference (Fig. 2*C*).

Functional Characterization of the *UHRF1* K667N Substitution in a Mouse Model. To evaluate the candidacy of the *UHRF1:* c.2001G>C, p.(Lys667Asn) (K667N) missense variant as a cause for BWSp with MLID, we used a CRISPR/Cas9 strategy to create the equivalent substitution [*Uhrf1* K661N in exon 15 (GRCm39: chr17:56627428)] and generated a transgenic mouse model (Fig. 3*A*). To create a restriction enzyme (RE) site for genotyping, a silent mutation was also introduced 9 base pairs upstream (Fig. 3*A*). The presence of the K661N variant was confirmed by Sanger sequencing (*SI Appendix*, Fig. S1*B*).

Postnatal phenotyping studies. To investigate whether mice homozygous for the K661N variant might display BWSp features such as postnatal overgrowth, macroglossia, and anterior abdominal wall defects postnatal studies were performed measuring body weights and organ weights of wild type ($Uhrf1^{+/+}$), heterozygous ($Uhrf1^{+/G>C}$), and homozygous ($Uhrf1^{G>C/G>C}$) mice from double-heterozygous crosses. Body and organ weights at birth (P1) were similar between all genotypes (*SI Appendix*, Fig. S2 *A* and *B*). No evidence of macroglossia or anterior abdominal wall defects was detected. Postnatal growth curves over 11 wk did not reveal significant weight differences between genotypes (*SI Appendix*, Fig. S2*C*), with body weight, fat, and lean mass being similar between genotypes in 12-wk-old males and females (*SI Appendix*, Fig. S2 *D–I*). Comparison of the number of pups born to double wild-type, double heterozygous, and double homozygous crosses revealed significant differences in the number of pups at P1. Thus, the mean number of pups per litter at P1 for double wild type, double heterozygous, and double homozygous crosses was 7.9 [Number pups (n) = 63, Number of litters (N) = 8], 7.8 (n = 70, N = 9) and 2.0 (n = 26, N = 13), respectively (*SI Appendix*, Table S3). These results suggested potential prenatal lethality in P1 offspring from homozygous mothers. Accordingly, the loss of neonates is only observed when the mother, but not the father, is homozygous (Fig. 3*B* and *SI Appendix*, Table S3).

Prenatal phenotyping. To determine the gestational stage when developmental alterations/embryonic lethality occurred, we studied embryos at E11, E14, and E17 (*SI Appendix*, Table S3).

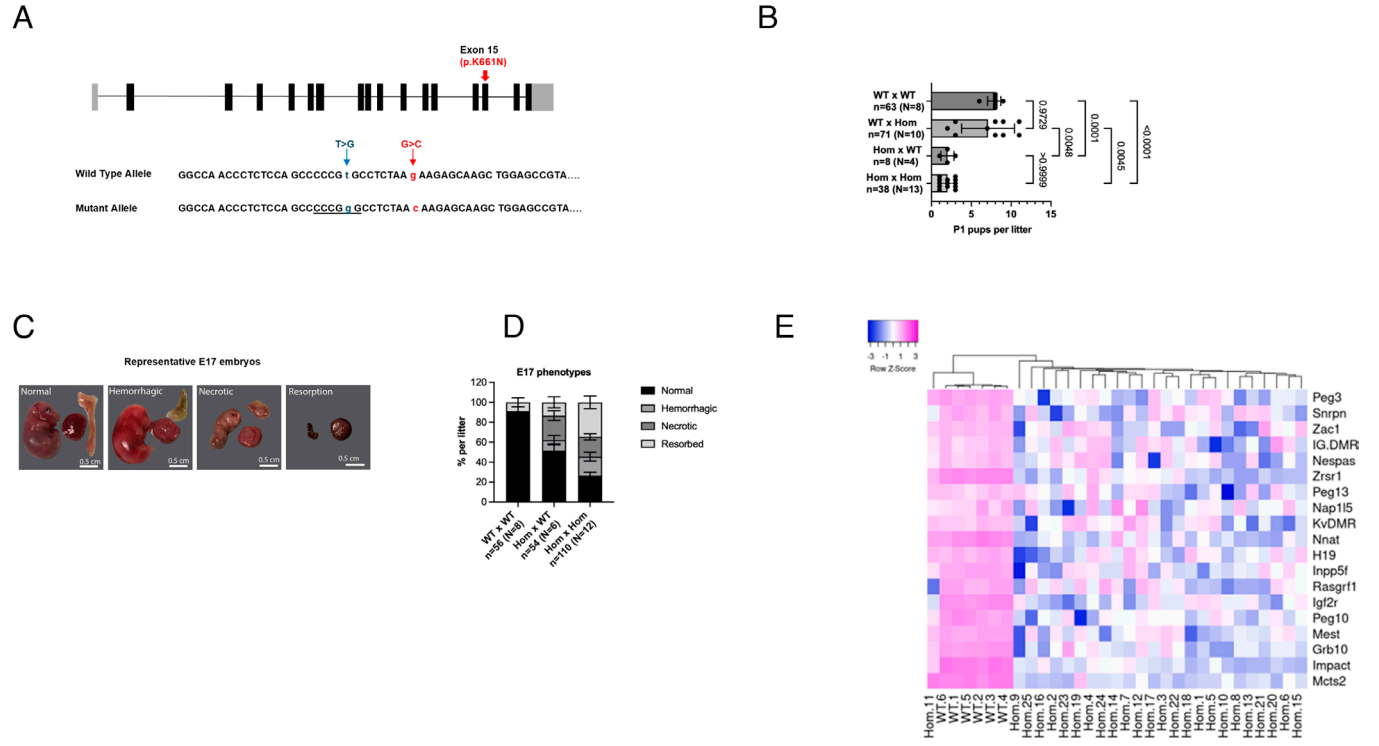

Fig. 3. Details of a mouse model of the *UHRF1* missense substitution. (*A*) A point mutation was introduced into *Uhrf1* by CRISPR–Cas9 technique. (*B*) P1 offspring from homozygous mothers displayed partial lethality. Error bars represent SD. (*C*) Mice from homozygous mothers displayed developmental defects and showed partial embryonic lethality at E17. (*D*) Relative percentages of E17 embryos presenting with phenotypes shown in *C* from different types of crosses; Error bars represent SEM. (*E*) Unsupervised hierarchical clustering and heatmaps of 19 ICRs from pyrosequencing analysis (percent CpG methylation) for $Uhrf1^{G>C/G>C}$ and $Uhrf1^{+/+}$ s-E11 embryos. Color coding is as per legend and indicates the row Z-score. The clustering and the visualization of the results from the pyrosequencing analysis (percent CpG methylation) were performed using the web-based tool Heatmapper (http://www.heatmapper.ca/expression/).

The mean number of embryos per litter in double wild type crosses per developmental stage (E11, E14, and E17) was 8.7 (n = 26, N = 3), 9.0 (n = 63, N = 7), and 7.0 (n = 61, N = 8), respectively. In double homozygous crosses, the mean number of embryos per litter per developmental stage (E11, E14, and E17) was 7.6 (n = 61, N = 8), 6.4 (n = 72, N = 9), and 2.5 (n = 110, N = 12), respectively. These results indicated a reduction in the number of embryos per litter in all stages in double homozygous crosses in comparison with double wild type. But the effect was most pronounced at E17 developmental stage (*SI Appendix*, Table S3). Significant embryonic losses at E17 were observed when the mothers were homozygous but not if they were heterozygous (*SI Appendix*, Table S3).

Embryos from double homozygous crosses displayed a wide range of developmental defects at E17 (Fig. 3*C*). Embryos from double homozygous crosses (n = 110, N = 12) and from homozygous mother crossed with wild-type males (n = 54, N = 6) had a higher proportion of haemorrhagic, necrotic, and reabsorbed phenotypes (Fig. 3*D* and *SI Appendix*, Fig. S3), despite appearing normal at E11 and E14 (*SI Appendix*, Table S3). In contrast, embryos from homozygous fathers' crosses with heterozygous or wild-type mothers showed no evidence for developmental phenotypes and were indistinguishable from double wild-type crosses (*SI Appendix*, Table S3).

Methylation profiling in E11 embryos from homozygous mutant mothers. To determine whether the embryonic lethality that was most pronounced at E17 might be a consequence of genomic methylation alterations present at an earlier stage of pregnancy, we undertook RRBS experiments on whole embryos at E11 from double homozygous crosses (n = 10) and double wild type crosses (n = 9). After filtering, 991,858 CpGs across the mouse genome were retained for the comparison of DNA methylation profiles between double homozygous crosses and double wild type crosses. The results revealed no significant alterations on DNA methylation between crosses with *P*-value adjusted <0.05. Considering that whole embryos containing tissues with different DNA methylation profiles were analyzed, we considered significant also those alterations with p-value unadjusted <0.01, level change >10% and more than 1 CpG per region. Based on these criteria, we identified 11 CpG islands (all hypomethylated) that showed significant DNA methylation alterations between crosses at E11 (*SI Appendix*, Table S4). From these regions 10 out of 11 CpGi *(Mcts2, Airn, Znf777, Znf444, Kcnq1ot1, Nnat, Zrsr1, Impact, Plagl1, Zfp787*) were located within IR (Dataset S2). The findings that E11 embryos born to homozygous *Uhrf1* variant mothers showed frequent LOM at iDMRs were further validated by pyrosequencing analysis (n = 6 wild-type embryos; n = 25 homozygous embryos) at ICRs (Fig. 3*E*). This extended analysis shows that embryos are variably and stochastically affected, with several embryos showing relative retention of DNA methylation at ICRs.

Discussion

Here, we described two siblings from a family with parental consanguinity who were diagnosed with BWSp and displayed extensive MLID. Approximately 25% of individuals with BWSp and LOM at IC2 will demonstrate MLID (19, 33, 34). Previously, MLID was defined as the presence of a HMA (either LOM or GOM) at least two CID-associated iDMR or at one CID iDMR and two non-CID iDMRs (33). However, there was extensive MLID in both siblings (III-1 and III-2) with significant methylation alterations (HMAs) at 26 iDMRs (25 LOM and 1 GOM), including LOM at KCNQ1OT1:TSS DMR (IC2). In a previous report of 147 individuals with CIDs assessed for MLID by ImprintSeq profiling, the most extreme MLID (26 HMAs) was detected in a child with atypical SRS whose mother had biallelic *PADI6* variants (33). Therefore, a genetic cause for the extreme MLID in III-1 and III-2 was suspected. A homozygous missense substitution [c. 2001G>C, p.(Lys667Asn/K667N)] was detected in both siblings and was present in the heterozygous state in both parents. This variant was extremely rare in reference populations, and the Lysine residue was highly conserved through evolution.

UHRF1 is a multidomain nuclear protein that acts as a key epigenetic regulator connecting DNA methylation and chromatin modifications. UHRF1 is essential for maintaining DNA methylation through recognizing and binding hemimethylated DNA at replication forks and recruiting the DNMT1 maintenance methyltransferase (35, 36). In addition, UHRF1 binds to histone H3 trimethylated at Lys-9 (H3K9me3) and H3 unmethylated at Arg-2 (H3R2me0) and is thought to mediate the recruitment of other factors to chromatin (37, 38). Uhrf1 has been implicated in both de novo DNA methylation in oocytes and in methylation maintenance in preimplantation embryos (39). Therefore, *UHRF1* appeared to be an excellent candidate gene for causing a CID with MLID [subsequently UHRF1 has been shown to interact with the core SCMC proteins NLRP5 and OOEP (40)] and computational predictions included both likely pathogenic and variant of uncertain significance and formal variant interpretation categorization according to ACMG/AMP guidelines resulted in "uncertain significance" classification (41). Though *UHRF1* has been considered a candidate gene for MLID susceptibility, at the time of the finding, there have been no confirmed reports of *UHRF1*-associated human disease with only a single case of a child with SRS and a MLID phenotype and a heterozygous p.(Val-172Met) variant that did not segregate with disease status (also present in mother and unaffected twin) (42). Therefore, to evaluate our hypothesis, we sought evidence that the K667N would impair UHRF1 function through in vivo modeling. Previously *Uhrf1* knockout (KO) mice were reported to die in early gestation with growth retardation and various malformations. Yet, *Uhrf1* KO mouse embryonic stem cells are viable and able to self-renew but display marked global DNA hypomethylation, delayed cell cycle progression, altered chromatin structure, and enhanced transcription of repetitive elements (35, 43, 44). We hypothesized that the K667N variant may be a hypomorphic variant causing partial loss of UHRF1 function and, having engineered the equivalent substitution (K661N) into the mouse germline, we were able to breed viable mice homozygous for the K661N variant. However, in contrast to humans homozygous for the K667N variant, the mice showed no clear phenotype. Nevertheless, further experiments demonstrated a disturbance of Uhrf1 function as evidenced by embryonic lethality in the offspring of female K661N homozygous mice. Furthermore, embryonal developmental defects were preceded by widespread iDMR methylation abnormalities. These findings supported the pathogenicity of the *UHRF1* K667N variant and our hypothesis that hypomorphic variants in *UHRF1* can cause an autosomal recessively inherited human CID associated with MLID. We note that there are two other autosomal recessive inherited causes of CID associated with MLID, *ZFP57* and *ZFP445*. Biallelic pathogenic variants in *ZFP57* are associated with TNDM (15) and not with other CIDs, though the phenotype of affected children can overlap with that of BWSp (13, 45). We note that in a *Zfp57* mouse KO model, homozygous mice demonstrated partial neonatal lethality, whereas *Zfp57* homozygotes born to *Zfp57*-deficient mothers demonstrated highly penetrant embryonic lethality (46). Therefore, though, to date, in humans, only a zygotic phenotype has been reported with defects

in ZFP57 function, in mice, both maternal and zygotic functions of Zfp57 are apparent. In mice Zfp445 and Zfp57 cooperate to regulate normal imprinting by maintaining methylation patterns at iDMRs (47). Interestingly, a single patient with Temple syndrome and severe MLID was found to harbor a homozygous truncating variant in *ZNF445* (48) and it has been suggested that ZNF445 and ZFP57 have differing roles maintaining genomic imprinting states in humans and mice (47). We found that the K661N variant in mice resulted in a maternal-effect disruption of imprinting whereas the effect is zygotic in humans. The maternal effect we observed in mice is consistent with the studies of report of oocyte-specific *Uhrf1* gene KO mice which revealed that oocyte-derived maternal Uhrf1 protein was important for CG maintenance methylation in preimplantation embryos, particularly at the imprinting control regions (ICR) (49). Furthermore, The zygotic effect in humans is consistent with the recent report by Unoki et al. (50) of a patient diagnosed with Immunodeficiency-Centromeric instability-Facial anomalies (ICF) syndrome without evidence of germline *DNMT3B* variants who harbored compound heterozygous variants in *UHRF1* [c.886C>T (p.Arg296Trp)/(R296W) and c.1852C>T (p.Arg618*)]. The combination of a plausible loss of function nonsense variant and a rare missense variant predicted to disrupt the function and structure of UHRF1 was considered to be likely to result in defective UHRF1-mediated regulation of genome methylation. Indeed, methylation profiling demonstrated abnormal DNA methylation with predominantly genomic hypomethylation. The pattern of DNA hypomethylation included centromeric/pericentromeric hypomethylation (a feature of ICF syndrome) but also other regions that were not typical of ICF syndrome. Interestingly, there were 61 imprinted genes associated with regions of hypomethylation. The observations of Unoki et al. (50) are consistent with the premise that biallelic pathogenic variants in *UHRF1* can cause an epigenetic disorder characterized by predominant genome hypomethylation. The difference in phenotypes between the BWSp-MLID seen in the current report and ICF syndrome by Unoki et al. (50) might result from allelic heterogeneity with differential effects on iDMR methylation or random epigenetic variability. The observed interspecies differences (maternal-effect versus zygotic) in the effects of *UHRF1/Uhrf1* disruption may reflect the importance of maternal expression of UHRF1 in early maintenance methylation such that in mice maternal Uhrf1 can compensate for the lack of zygotic Uhrf1 in homozygous mutants born to heterozygous mothers but in humans this is not the case. Extrapolating from the variable phenotypes, such as pregnancy loss, hydatidiform mole, and CIDs. reported in the pregnancies of women with biallelic maternal effect SCMC gene mutations, it is possible that MLID associated with pathogenic variants in *UHRF1* could also present with a range of different phenotypes. A major challenge in rare disease genetics is assessing the functional significance of rare missense variants without laborious experimental validation of the predicted effects on function. For candidate trans-acting genomic imprinting disorder genes, this is particularly challenging as experimental validation can require in vivo validation of the effects on reproduction. However, our findings and those of Unoki et al. (50) provide a framework for facilitating the assessment of candidate *UHRF1* variants by predicting the likely inheritance and candidate clinical and epigenetic phenotypes of *UHRF1*-associated human diseases. The rarity of polymorphic variation in *UHRF1* will reduce the number of candidate patients with biallelic variants and the occurrence methylation profiling could also inform the likelihood of a *UHRF1*-associated disorder. We note that for the two siblings, we studied the majority of iDMRs affected by MLID were common to both siblings. This differs somewhat from what has been described in the offspring of women with maternal effect gene mutations for whom the MLID patterns can be more variable (51) and raises the possibility of a *UHRF1*-associated episignature that could be used to inform the pathogenicity of variants of uncertain significance (as described for a growing number of chromatin disorder genes (52).

The methylation profiling we undertook in human and mice revealed that disruption of *UHRF1/Uhrf1* function via the K667N/K661N substitution preferentially impacted on iDMRs compared to methylation at nonimprinted loci. K667 is located between the SET and RING-associated (SRA) domain which recognizes 5-methylcytosine in hemimethylated DNA and the RING domain with E3 ligase activity which regulates ubiquitylation at H3K14, H3K18, and H3K23 residues (53–55). These ubiquitin marks are critical for DNMT1 binding via the ubiquitin-interacting motif and increase enzymatic activity in vitro (56, 57). Assuming that the missense substitution is causing a partial loss of UHRF1 efficacy, this could suggest that iDMRs are more sensitive to impaired UHRF1/Uhrf1 function than nonIR in a similar way to that described for ZFP57/Zfp57 (58, 59). Alternatively, the mutation could impact on an iDMR-selective function of UHRF1/Uhrf1. Intriguingly, it has been suggested recently that the pathogenicity of maternal biallelic mutations in SCMC-related genes is dependent on the function of UHRF1 and our findings could be consistent with this hypothesis (40, 60). Our findings suggest that germline variants in *UHRF1* should be further evaluated in individuals with MLID and no identifiable genetic cause.

Materials and Methods

Sex as a Biological Variable. Our study examined male and female mice, and sex-dimorphic effects are reported (parent of origin effects as a consequence of genomic imprinting).

Human Samples. Genomic DNA was extracted from peripheral blood using Gentra Puregene Blood Kit (Qiagen) or other standard methods and quantified by Qubit™ dsDNA BR Assay Kit (Invitrogen, ThermoFisher).

Whole-Exome Sequencing in Human Samples. Whole-exome sequencing was performed on three individuals. Bcl2fastq2 Conversion Software (Illumina, San Diego, CA) was used to generate demultiplexed FASTQ files. All samples were aligned to the human reference genome (GRCh38) version using bwa 0.7.15, the generated SAM file was compressed into a BAM file and sorted by genomic position using samtools 1.3.1 and variant calling was performed using Genome Analysis Toolkit 3.7 software (61, 62). All variants with a Q phred scaled quality score lower than 30 and a read depth lower than 30 were excluded from further analysis (best practice recommendation). The generated VCF files were manipulated using VCFTools 0.1.13 (63) and annotated using ANNOVAR and Variant Effect Predictor V109 (64).

Targeted and Genome Wide Methylation Profiling.

iDMR profiling in human samples. The methylation status of 63 iDMRs was interrogated using ImprintSeq, a hybridization-based custom panel of 3,989 probes covering >9,257 CpGs (33). Libraries were prepared as described previously and sequenced on an Illumina HiSeq4000 sequencing machine (Illumina, San Diego, CA) by the staff at the Stratified Medicine Core Laboratory within the Department of Medical Genetics, Cambridge University. The bcl files produced were demultiplexed into FASTQ files using Illumina's bcl2fastq v2.19 (Illumina, San Diego, CA) and, after demultiplexing, the quality of the sequencing data was assessed by FastQC software. After adapter removal, quality filtering, and further reevaluation by FastQC, data were aligned with human build hg19, PCR duplicates were removed, and methylation information was extracted using the Bismark software (65). We filtered out from the analysis any CpG with less than 100 reads of coverage to achieve accurate DNA methylation measurements. Correction of the methylation levels (fraction of methylated reads over total reads) for both cases and healthy controls

was performed using MethylCal (66). After correcting the observed methylation levels, we calculated the median of the methylation levels across CpGs (median methylation level or MML hereafter) for each individual and each DMR. For each DMR, patients with an MML below the healthy controls' 3SDs CI were considered to undergo LOM and those with a level above the same healthy controls' 3SDs CI were considered to experience GOM. Then, we divided significant LOM/GOM events into two groups according to the magnitude of the alteration in the differential median methylation level (DMML) between healthy controls and patients: high values of DMML (HMA) and moderate values of DMML (MMA).

Genome-wide methylation profiling in human and mouse samples by RRBS. RRBS libraries were prepared using the Ovation RRBS Methyl-Seq System (NuGEN), according to the manufacturer's recommendations. Briefly, 100 ng of purified DNA was digested with MspI enzyme followed by adaptor ligation and ends repair. Then, libraries were bisulfite converted, using the Qiagen Epitect kit, and amplified by PCR. The pooled library was normalized to 4 nM and sequenced in a lane of Illumina HiSeq4000 sequencing machine (Illumina, San Diego, CA) by the staff at the Stratified Medicine Core Laboratory within the Department of Medical Genetics, Cambridge University. The bcl files were demultiplexed into FASTQ files using Illumina's bcl2fastq v2.19 (Illumina, San Diego, CA), and the quality of the sequencing data was assessed by FastQC software. Then, adapter removal and low base quality filtering were performed with Trim_galore (--paired -a AGATCGGAAGAGC -a2 AAATCAAAAAAAC -q 20) (https://github.com/FelixKrueger/TrimGalore). To preserve the first base of the MspI fragment, which contains a CpG methylation measurement, we trimmed diversity sequence (0 to 3 bases) on the 5′ end and 5 bases on the 3′ end using NuGen in-house python script trimRRBSdiversityAdaptCustomers. After reevaluating quality by FastQC, data were aligned with human build hg19 and mouse build mm10 using bismark software (65). Before PCR duplicates were removed using NuGen in-house python script NuDup, bismark alignment output files were modified for NuDup using NuGen in-house bash script strip_bismark_sam. Finally, methylation was extracted with bismark_methylation_extractor included in bismark software (65). Bioinformatic guidelines and in-house scripts for Ovation RRBS Methyl-Seq System can be found at https://github.com/nugentechnologies/NuMetRRBS. Quality control and CpG filtering of bismark coverage files were performed with RnBeads 2.0 package (67, 68). CpGs that overlap with SNPs, with high coverage outliers in at least one sample, with coverage below 10 and with missing values in at least one sample were removed for further analyses. Differential methylation analyses adjusted by sex between cases and control were also performed with RnBeads 2.0 package (67, 68).

Generation of the Uhrf1 K661N Mouse Model. We targeted *Uhrf1* to introduce a point mutation at the Lysine residue 661 (GRCm39 transcript ID ENSMUST00000001258.15, G > C position 17:56627428 in exon 15 ID ENSMUSE00001311486) by pronuclear injection using CRISPR/Cas9 gene editing technology (Fig. 3*A* and *SI Appendix*, Fig. S1). Briefly, one-cell stage C57Bl/6J embryos were injected with 30 ng/μL Cas9 protein, 0.61 pmol/μl annealed CRISPR RNA (crRNA) and Trans-activating CRISPR RNA (tracrRNA) (TRACRRNA05N, Sigma-Aldrich), and 10 ng/μL single-stranded donor oligo. The sequence of the crRNA guide 5′-3′ with PAM (underlined) was CTTGCTCTTCTTAGAGGCACGG. The sequence of the 132 bp donor oligo was 5′-3′: TCCTCACTGCCTTGTTCTACCTCCT CCTGACTCCCCACAGGGCCAACCCTCTCCAGCCCCCGgGCCTCTAAcAAGAGCAAGC TGGAGCCGTACACACTCTCAGAGCAGCAGGCTAACCTCATCAAAGAGGAC. To facilitate genotyping, a silent mutation T > G creating a SmaI RE site was also introduced at position 17:56627420 (GRCm39) (*SI Appendix*, Fig. S1 *A* and *B*).

Injected embryos were transferred the same day into the oviducts of pseudo-pregnant F1 (C56BL/6J/CBA) recipients. The resulting F0 male founder that was a carrier of both the silent and the desired mutation was crossed with wild-type C57BL/6J females (Charles River) to generate F1 mice. Mutations in F0 and F1 mice were confirmed by Sanger sequencing (*SI Appendix*, Fig. S1*B*).

To exclude the unintended side effects from possible CRISPR off-targets, the genomic DNA extracted from three F1 founders was analyzed. The CRISPR Finder tool (Wellcome Sanger Institute Genome editing–WGE) was employed to predict the off-target candidate loci. 31 loci with 1, 2, and 3 mismatches were amplified by PCR and analyzed by Sanger sequencing. No off-target mutations were found. Founder F1 mice were then crossed with wild-type C57BL/6J mice, thus establishing the experimental F2 mouse colony (*SI Appendix*, Fig. S1*C*).

Mouse Genotyping. Mice (ear biopsies, embryonic tissues) were genotyped using standard PCR with Phusion polymerase and primers 190F (5′-GGTGCTAGGGTAGGACCTCTTT-3′) and 191R (5′-AGTGCTGCAGTAGGACAGACAG-3′) (*SI Appendix*, Fig. S1D); PCR conditions were as follows: 98 °C for 30 s for 1 cycle, then (98 °C for 5 s, 66 °C for 5 s, 72 °C for 19 s) for 29 cycles, and 72 °C for 5 min. PCR products were digested with SmaI and separated on 1.5% agarose gel.

Mouse Phenotyping. For embryonic and neonatal studies, wild-type C57Bl/6J, *Uhrf1*$^{+/G>C}$ (heterozygous), and *Uhrf1*$^{G>C/G>C}$ (homozygous) females were set up with either wild-type C57Bl/6J, *Uhrf1*$^{+/G>C}$ or *Uhrf1*$^{G>C/G>C}$ males and housed overnight. Successful mating was evaluated the following morning by the presence of a vaginal plug (considered as embryonic day E0). Embryos and neonatal organs from the various crosses were collected at E11, E14, E17, and P1, weighed, and snap-frozen for DNA extractions.

For postnatal studies, mice homozygous for the mutation (*Uhrf1*$^{G>C/G>C}$) were born from heterozygous intercrosses and used for phenotypic analyses in parallel with age- and sex-matched wild-type and heterozygous littermates. Whole body weights were measured on a weekly basis.

Body composition analysis was performed in 12-wk-old mice by time-domain NMR spectroscopy that measures total body fat mass and lean mass. For this purpose, live and conscious mice were placed inside the Minispec Live Mice Analyser (Bruker Minispec Live Mice Analyser LF50). Organ wet weights were then measured after dissection at 12 wk.

Mouse Methylation Assays. Bisulfite pyrosequencing was performed as previously described in Bertozzi et al. (69). The sequence of the primers used is shown in *SI Appendix*, Table S1.

Study Approval. Human participants: The study was approved by the South Birmingham Research Ethics Committee and written informed consent was obtained for all participants. The investigations were conducted according to Declaration of Helsinki principles. The mice studies were regulated under the Animals (Scientific Procedures) Act 1986 Amendment Regulations 2012 following ethical review and approval by the University of Cambridge Animal Welfare and Ethical Review Body.

Data, Materials, and Software Availability. The data for the mouse methylation studies underlying this article are available in NCBI/NLM Sequence Read Archive (SRA) submission number SUB11164966 (70). Anonymized human sequencing data are available from the European Genome Phenome Archive (dataset ID EGAD50000001684) upon publication (71).

ACKNOWLEDGMENTS. This research was cofunded by the National Institute for Health and Care Research Cambridge Biomedical Research Centre (BRC-1215-20014) and Rosetrees Trust (to E.O., S.L., and E.R.M.), Marie Curie Initial Training Network Award (INGENIUM) (B.L.-L., E.R.M.), from the European Union, Alan Turing Institute under the Engineering and Physical Sciences Research Council [EP/N510129/1 to L.B.], King Abdullah University of Science and Technology [OSR-GRG2019-4043 to W.F., M.C., and E.R.M.] Medical Research Council [MRC_MC_UU_12012/4 to M.C.; MRC_MC_UU_12012/5 to the Medical Research Council Metabolic Diseases Unit] and EpiGenRare Medical Research Council Rare Diseases Node funding MR/Y008170/1 to E.R.M.]. Funding for open access charge: Cambridge Open Access: https://www.openaccess.cam.ac.uk/. The views expressed are those of the authors and not necessarily those of the National Health Service or Department of Health. We acknowledge the support from the National Institute for Health and Care Research UK Rare Genetic Disease Research Consortium.

Author affiliations: [a]Department of Genomic Medicine, University of Cambridge and National Institute for Health and Care Research Cambridge Biomedical Research Centre, Cambridge CB2 0QQ, United Kingdom; [b]Wellcome-Medical Research Council Institute of Metabolic Science and Medical Research Council Metabolic Diseases Unit, University of Cambridge, Cambridge CB2 0QQ, United Kingdom; [c]Department of Genetics, University of Cambridge, Cambridge CB2 3EH, United Kingdom; [d]Leeds Clinical Genomics Service, Chapel Allerton Hospital, Leeds Teaching Hospitals National Health Service Trust, Leeds LS7 4SA, United Kingdom; [e]Stratified Medicine Core Laboratory Next Generation Sequencing Hub, Cambridge CB2 0QQ, United Kingdom; [f]Department of Obstetrics and Gynaecology and National Institute for Health Research Cambridge Biomedical Research Centre, Cambridge CB2 0SW, United Kingdom; [g]The Alan Turing Institute, London NW1 2DB, United Kingdom; [h]Medical Research Council Biostatistics Unit, University of Cambridge, Cambridge CB2 0QQ, United Kingdom; [i]Bioscience Program, Biological and Environmental Science and Engineering Division, King Abdullah University of Science and Technology, Thuwal 23955, Kingdom of Saudi Arabia; [j]Centre for Trophoblast Research, Department of Physiology, Development and Neuroscience, University of Cambridge, Cambridge CB2 3EG, United Kingdom; and [k]Aston Medical School, College of Health and Life Sciences, Aston University, Birmingham B4 7ET, United Kingdom

1. J. Peters, The role of genomic imprinting in biology and disease: An expanding view. *Nat. Rev. Genet.* **15**, 517–530 (2014).
2. D. Monk, D. J. G. Mackay, T. Eggermann, E. R. Maher, A. Riccio, Genomic imprinting disorders: Lessons on how genome, epigenome and environment interact. *Nat. Rev. Genet.* **20**, 235–248 (2019).
3. W. Reik, W. Dean, J. Walter, Epigenetic reprogramming in mammalian development. *Science* **293**, 1089–1093 (2001).
4. D. M. Messerschmidt, B. B. Knowles, D. Solter, DNA methylation dynamics during epigenetic reprogramming in the germline and preimplantation embryos. *Genes Dev.* **28**, 812–828 (2014).
5. M. A. Eckersley-Maslin, C. Alda-Catalinas, W. Reik, Dynamics of the epigenetic landscape during the maternal-to-zygotic transition. *Nat. Rev. Mol. Cell Biol.* **19**, 436–450 (2018).
6. F. Zink *et al.*, Insights into imprinting from parent-of-origin phased methylomes and transcriptomes. *Nat. Genet.* **50**, 1542–1552 (2018).
7. T. Eggermann *et al.*, Imprinting disorders: A group of congenital disorders with overlapping patterns of molecular changes affecting imprinted loci. *Clin. Epigenet.* **7**, 123 (2015).
8. T. Eggermann *et al.*, Imprinting disorders. *Nat. Rev. Dis. Primers* **9**, 33 (2023).
9. A. Ibrahim *et al.*, Methylation analysis and diagnostics of Beckwith-Wiedemann syndrome in 1, 000 subjects. *Clin. Epigenet.* **6**, 11 (2014).
10. F. Brioude *et al.*, Expert consensus document: Clinical and molecular diagnosis, screening and management of Beckwith-Wiedemann syndrome: An international consensus statement. *Nat. Rev. Endocrinol.* **14**, 229–249 (2018).
11. E. L. Wakeling *et al.*, Diagnosis and management of Silver–Russell syndrome: First international consensus statement. *Nat. Rev. Endocrinol.* **13**, 105–124 (2017).
12. M. Sanchez-Delgado *et al.*, Causes and consequences of multi-locus imprinting disturbances in humans. *Trends Genet.* **32**, 444–455 (2016).
13. T. Eggermann *et al.*, Trans-acting genetic variants causing multilocus imprinting disturbance (MLID): Common mechanisms and consequences. *Clin. Epigenet.* **14**, 41 (2022).
14. L. Tee *et al.*, Epimutation profiling in Beckwith-Wiedemann syndrome: Relationship with assisted reproductive technology. *Clin. Epigenet.* **5**, 23 (2013).
15. D. J. G. Mackay *et al.*, Hypomethylation of multiple imprinted loci in individuals with transient neonatal diabetes is associated with mutations in ZFP57. *Nat. Genet.* **40**, 949–951 (2008).
16. E. Meyer *et al.*, Germline mutation in *NLRP2* (*NALP2*) in a familial imprinting disorder (Beckwith-Wiedemann syndrome). *PLoS Genet.* **5**, e1000423 (2009).
17. L. E. Docherty *et al.*, Mutations in *NLRP5* are associated with reproductive wastage and multilocus imprinting disorders in humans. *Nat. Commun.* **6**, 8086 (2015).
18. P. Tannorella *et al.*, Germline variants in genes of the subcortical maternal complex and multilocus imprinting disturbance are associated with miscarriage/infertility or Beckwith-Wiedemann progeny. *Clin. Epigenet.* **14**, 43 (2022).
19. L. Bilo *et al.*, Molecular characterisation of 36 multilocus imprinting disturbance (MLID) patients: A comprehensive approach. *Clin. Epigenet.* **15**, 35 (2023).
20. T. Eggermann, Maternal effect mutations: A novel cause of human reproductive failure. *Geburtshilfe Frauenheilkd.* **81**, 780–788 (2021).
21. H. Sidhu, N. Capalash, UHRF1: The key regulator of epigenetics and molecular target for cancer therapeutics. *Tumour Biol.* **39**, 1–11 (2017).
22. X. Liu *et al.*, UHRF1 targets DNMT1 for DNA methylation through cooperative binding of hemi-methylated DNA and methylated H3K9. *Nat. Commun.* **4**, 1563 (2013).
23. A. C. Berkyurek *et al.*, The DNA methyltransferase Dnmt1 directly interacts with the SET and RING finger–associated (SRA) domain of the multifunctional protein Uhrf1 to facilitate accession of the catalytic center to hemi-methylated DNA. *J. Biol. Chem.* **289**, 379–386 (2014).
24. S. Chen *et al.*, A genomic mutational constraint map using variation in 76,156 human genomes. *Nature* **625**, 92–200 (2024).
25. J. M. Schwarz *et al.*, Mutationtaster2: Mutation prediction for the deep-sequencing age. *Nat. Methods* **11**, 361–362 (2014).
26. P. C. Ng, S. Henikoff, SIFT: Predicting amino acid changes that affect protein function. *Nucleic Acids Res.* **31**, 3812–3814 (2003).
27. I. A. Adzhubei *et al.*, A method and server for predicting damaging missense mutations. *Nat. Methods* **7**, 248–249 (2010).
28. P. Rentzsch, D. Witten, G. M. Cooper, J. Shendure, M. Kircher, CADD: Predicting the deleteriousness of variants throughout the human genome. *Nucleic Acids Res.* **47**, D886–D894 (2019).
29. W. G. McLaren, *et al*., The Ensembl Variant Effect Predictor. *Genome Biol.* **17**, 122 (2016).
30. N. M. Ionnadis *et al.*, Revel: An ensemble method for predicting the pathogenicity of rare missense variants. *Am. J. Hum. Genet.* **99**, 877–885 (2016).
31. P. Katsonis, O. Lichtarge, Meta-ea: A gene-specific combination of available computational tools for predicting missense variant effects. *Nat. Commun.* **16**, 159 (2025).
32. J. Cheng *et al.*, Accurate proteome-wide missense variant prediction with AlphaMissense. *Science* **381**, eadg7492 (2023).
33. E. Ochoa *et al.*, Imprintseq, a novel tool to interrogate DNA methylation at human imprinted regions and diagnose multilocus imprinting disturbance. *Genet. Med.* **24**, 463–474 (2022).
34. S. Rossignol *et al.*, The epigenetic imprinting defect of patients with Beckwith-Wiedemann syndrome born after assisted reproductive technology is not restricted to the 11p15 region. *J. Med. Genet.* **43**, 902–907 (2006).
35. M. Bostick *et al.*, UHRF1 plays a role in maintaining DNA methylation in mammalian cells. *Science* **317**, 1760–1764 (2007).
36. J. Sharif *et al.*, The SRA protein Np95 mediates epigenetic inheritance by recruiting Dnmt1 to methylated DNA. *Nature* **450**, 908–912 (2007).
37. L. Hu, Z. Li, P. Wang, Y. Lin, Y. Xu, Crystal structure of PHD domain of UHRF1 and insights into recognition of unmodified histone H3 arginine residue 2. *Cell Res.* **21**, 1374–1378 (2011).
38. E. Rajakumara *et al.*, PHD finger recognition of unmodified histone H3R2 links UHRF1 to regulation of euchromatic gene expression. *Mol. Cell* **43**, 275–284 (2011).
39. S. Maenohara *et al.*, Role of UHRF1 in *de novo* DNA methylation in oocytes and maintenance methylation in preimplantation embryos. *PLoS Genet.* **13**, e1007042 (2017).
40. M. Unoki, S. Uemura, A. Fujimoto, H. Sasaki, The maternal protein NLRP5 stabilizes UHRF1 in the cytoplasm: Implication for the pathogenesis of multilocus imprinting disturbance. *Hum. Mol. Genet.* **33**, 1575–1583 (2024), 10.1093/hmg/ddae096.
41. S. Richards *et al.*, Standards and guidelines for the interpretation of sequence variants: A joint consensus recommendation of the American College of Medical Genetics and Genomics and the Association for Molecular Pathology. *Genet. Med.* **17**, 405–424 (2015).
42. M. Begemann *et al.*, Maternal variants in NLRP and other maternal effect proteins are associated with multilocus imprinting disturbance in offspring. *J. Med. Genet.* **55**, 497–504 (2018).
43. M. Muto *et al.*, Targeted disruption of Np95 gene renders murine embryonic stem cells hypersensitive to DNA damaging agents and DNA replication blocks. *J. Biol. Chem.* **277**, 34549–34555 (2002).
44. K. Y. Kim *et al.*, Uhrf1 regulates active transcriptional marks at bivalent domains in pluripotent stem cells through Setd1a. *Nat. Commun.* **9**, 2583 (2018).
45. S. E. Boonen *et al.*, No evidence for pathogenic variants or maternal effect of ZFP57 as the cause of Beckwith–Wiedemann syndrome. *Eur. J. Hum. Genet.* **20**, 119–121 (2012).
46. X. Li *et al.*, A maternal-zygotic effect gene, Zfp57, maintains both maternal and paternal imprints. *Dev. Cell* **15**, 547–557 (2008).
47. N. Takahashi *et al.*, ZNF445 is a primary regulator of genomic imprinting. *Genes Dev.* **33**, 49–54 (2019).
48. M. Kagami *et al.*, ZNF445: A homozygous truncating variant in a patient with Temple syndrome and multilocus imprinting disturbance. *Clin. Epigenet.* **13**, 119 (2021).
49. S. Maenohara *et al.*, Role of UHRF1 in *de novo* DNA methylation in oocytes and maintenance methylation in preimplantation embryos. *PLoS Genet.* **13**, e1007042 (2017).
50. M. Unoki *et al.*, Novel compound heterozygous mutations in UHRF1 are associated with atypical immunodeficiency, centromeric instability and facial anomalies syndrome with distinctive genome-wide DNA hypomethylation. *Hum. Mol. Genet.* **32**, 1439–1456 (2023).
51. L. Fontana *et al.*, Characterization of multi-locus imprinting disturbances and underlying genetic defects in patients with chromosome 11p15.5 related imprinting disorders. *Epigenetics* **13**, 897–909 (2018).
52. J. Kerkhof *et al.*, DNA methylation episignature testing improves molecular diagnosis of Mendelian chromatinopathies. *Genet. Med.* **24**, 51–60 (2022).
53. W. Qin *et al.*, DNA methylation requires a DNMT1 ubiquitin interacting motif (UIM) and histone ubiquitination. *Cell Res.* **25**, 911–929 (2015).
54. P. A. DaRosa *et al.*, A bifunctional role for the UHRF1 UBL domain in the control of hemi-methylated DNA-dependent histone ubiquitylation. *Mol. Cell* **72**, 753–765.e6 (2018).
55. B. M. Foster *et al.*, Critical role of the UBL domain in stimulating the E3 ubiquitin ligase activity of UHRF1 toward chromatin. *Mol. Cell* **72**, 739–752.e9 (2018).
56. A. Nishiyama *et al.*, Uhrf1-dependent H3K23 ubiquitylation couples maintenance DNA methylation and replication. *Nature* **502**, 249–253 (2013).
57. S. Ishiyama *et al.*, Structure of the Dnmt1 reader module complexed with a unique two-mono-ubiquitin mark on histone H3 reveals the basis for DNA methylation maintenance. *Mol. Cell* **68**, 350–360.e7 (2017).
58. R. Strogantsev *et al.*, Allele-specific binding of ZFP57 in the epigenetic regulation of imprinted and non-imprinted monoallelic expression. *Genome Biol.* **16**, 112 (2015).
59. V. Riso *et al.*, ZFP57 maintains the parent-of-origin-specific expression of the imprinted genes and differentially affects non-imprinted targets in mouse embryonic stem cells. *Nucleic Acids Res.* **44**, 8165–8178 (2016).
60. C. Giaccari *et al.*, A maternal-effect *Padió* variant causes nuclear and cytoplasmic abnormalities in oocytes, as well as failure of epigenetic reprogramming and zygotic genome activation in embryos. *Genes Dev.* **38**, 131–150 (2024).
61. A. McKenna *et al.*, The genome analysis toolkit: A MapReduce framework for analyzing next-generation DNA sequencing data. *Genome Res.* **20**, 1297–1303 (2010).
62. M. A. Depristo *et al.*, A framework for variation discovery and genotyping using next-generation DNA sequencing data. *Nat. Genet.* **43**, 491–501 (2011).
63. P. Danecek *et al.*, The variant call format and VCFtools. *Bioinformatics* **27**, 2156–2158 (2011).
64. W. McLaren *et al.*, The Ensembl variant effect predictor. *Genome Biol.* **17**, 122 (2016).
65. F. Krueger, S. R. Andrews, Bismark: A flexible aligner and methylation caller for Bisulfite-Seq applications. *Bioinformatics* **27**, 1571–1572 (2011).
66. E. Ochoa *et al.*, Methylcal: Bayesian calibration of methylation levels. *Nucleic Acids Res.* **47**, e81 (2019), 10.1093/nar/gkz325.
67. Y. Assenov *et al.*, Comprehensive analysis of DNA methylation data with RnBeads. *Nat. Methods* **11**, 1138–1140 (2014).
68. F. Müller *et al.*, Rnbeads 2.0: Comprehensive analysis of DNA methylation data. *Genome Biol.* **20**, 55 (2019).
69. T. M. Bertozzi, N. Takahashi, G. Hanin, A. Kazachenka, A. C. Ferguson-Smith, A spontaneous genetically induced epiallele at a retrotransposon shapes host genome function. *Elife* **10**, e65233 (2021).
70. S. Lee, Germline variants in UHRF1 are associated with multi locus imprinting disturbance in humans and mice. NCBI BioProject. https://www.ncbi.nlm.nih.gov/bioproject/PRJNA1302305. Deposited 6 August 2025.
71. S. Lee, Human exome sequencing data from the publication "Germline variants in UHRF1 are associated with multilocus imprinting disturbance in humans and mice". European Genome Phenome Archive [EGAD50000001684]. https://ega-archive.org/studies. Deposited 5 August 2025.